Uncovering seismic HTI anisotropy of the Cooper Basin

Stephanie Tyiasning*
The University of Adelaide
Adelaide
stephanie.tyiasning@adelaide.edu.au

Dennis Cooke
The University of Adelaide & ZDac Geophysical
Adelaide
dennis.cooke@adelaide.edu.au

SUMMARY

3D seismic data from the Cooper Basin exhibit horizontal transverse isotropy (HTI) anisotropy in amplitude versus offset (AVO) and interval migration velocity. Theoretically, vertical fractures and in-situ stress can induce HTI anisotropy. The main objective is to determine if the HTI anisotropy is caused by fractures or by the Cooper Basin's large difference between minimum and maximum horizontal stress. We compare migration velocity anisotropy and seismic AVO anisotropy extracted from a high-quality 3D survey with a "ground truth" of dipole sonic logs, borehole breakout, and fractures interpreted from image logs. The AVO anisotropy is inverted using Rüger AVO algorithm and Fourier Coefficient algorithm that give similar results. Fractures interpreted from image logs are primarily oriented approximately 30° from S_H.

Our work suggests that stress is the dominant cause of the HTI anisotropy observed in the seismic data. The fact that seismic anisotropy is parallel with current S_H and not aligned with the observed fractures suggests that Cooper Basin large differential stress causes the anisotropy observed on seismic.

Keywords: Anisotropy; in-situ stress; fractures; AVO; migration velocity.

INTRODUCTION

Understanding and mapping stress and natural fractures can be very important for unconventional reservoirs. Many authors have discussed how information about stress and fractures can be extracted from azimuthal anisotropy observed in 3D seismic data (Perez and Gibson Jr 1996, Sarkar, et al. 2003, Sayers and Rickett 1997). However, it is very difficult to define if anisotropy, in any case, is associated with stress or fractures. The main objective of this research is to find out if stress or fractures cause seismic anisotropy in the Cooper Basin. We extract anisotropy from 3D seismic data, which is then followed by a comparison of that anisotropy with dipole sonic logs, image log, cores and core plugs.

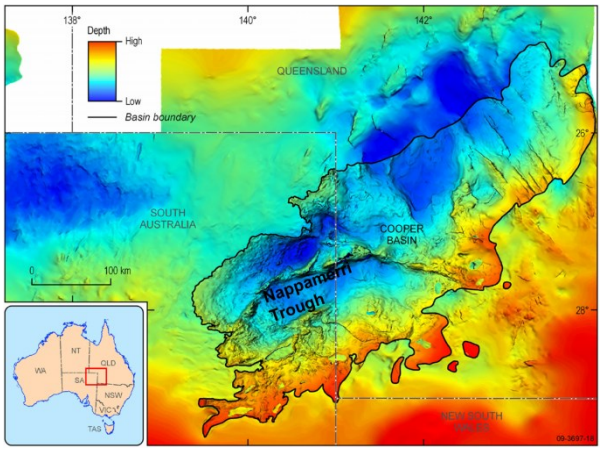

Figure 1: Modified map of the Cooper Basin (outlined by black lines) (Radke 2009). Colour bar corresponds to depth based on top Permian Toolachee Formation. Study area is situated in the Nappamerri Trough, however the exact location of the 3D survey area is confidential.

Our study area and data set may have some advantages over other basins in resolving the question: is seismic anisotropy caused by stress or fractures? Those advantages are: 1) many North American basins with unconventional reservoirs are in a normal stress regime where faults and fractures tend to be aligned with the maximum horizontal stress. The Cooper Basin is in a strike-slip regime, which leads to faults and fractures that are not aligned with maximum horizontal stress. 2) the high differential horizontal stress of the Cooper Basin leads to a maximum stress direction that does not vary significantly in orientation, 3) the Cooper Basin has good quality image logs, and 4) there is excellent fully azimuthal 3D seismic available.

STRESS AND ANISOTROPY

Geology and in situ stress

There are currently three different active unconventional plays in the Cooper Basin of Australia: a shale gas play, a deep coal play and a basin-centered tight gas sand play (Greenstreet and Dello 2015). This paper focuses on the Permian tight gas sand play in the Nappamerri Trough of the Cooper basin (Figure 1).

Cooper Basin in situ stress is strike-slip at shallow depth and transitions into reverse fault regime at depth (about 3km) while the principal maximum horizontal stress (S_H) direction is consistent at approximately N100°E (King, et al. 2011, Reynolds, et al. 2005). In our study area, the target Permian tight gas sand is at a depth of about 2.2 – 2.4km depth. Since these sands are expected to be in a strike-slip regime, we are expecting to see fractures oriented conjugate to the S_H direction as in Figure 2.

Velocity anisotropy

Stress and fractures cannot be directly measured on seismic data, but velocities extracted from seismic data are a function of stress and fractures. Mavko, et al. (1995) show ultrasonic P-wave (V_P) and S-wave velocities (V_S) on a dry granite sample increase with isotropic stress.

Before the emergence of unconventional reservoirs, geoscientists largely ignored anisotropy primarily because describing anisotropy was very cumbersome, and transverse isotropy (most common type of anisotropy) masquerades as isotropy in near-offset reflections (0-30°). Thomsen (1986) pointed out that 'in the case of weak anisotropy, describing anisotropy can be greatly simplified'. Geoscientists now routinely recognize vertical transverse isotropy (VTI) and horizontal transverse isotropy (HTI) in seismic data processing (Grechka and Tsvankin 1999, Jenner 2011, Treadgold, et al. 2008). Thin layering and lattice preferred orientation are responsible for VTI (Valcke, et al. 2006) while HTI can be caused by stress (Nur and Simmons 1969) and aligned vertical fractures (Sayers and Rickett 1997, Schoenberg and Sayers 1995). Figure 3 from Nur and Simmons (1969) shows a good example of anisotropic stress and velocity where compressional waves travel fastest in the direction of applied stress. Sayers and Rickett (1997) show how aligned vertical fractures affect azimuthal seismic amplitude from a gas sandstone while Schoenberg and Sayers (1995) present seismic modeling of fractured media.

For the purpose of understanding and calibrating the relationship between our 3D seismic velocities and stress, we use data from triaxial tests on Cooper Basin core plugs shown in Figure 3. This plug dataset does not measure velocities in multiple directions (all lines in Figure 3). Instead, it measures velocity in the direction of maximum stress over a range of differential stress (the first line of Figure 3, θ = 0°). The static measurements made on the core plugs include density, Poisson's ratio, and Young's modulus as a function of stress. Young's modulus was determined as the tangential slope of differential stress vs. average axial strain curve while the Poisson's ratio was the tangential slope of radial strain vs. axial strain curve. From these static elastic parameters, V_P was computed that was then converted to dynamic, well-logging velocity using an average scale factor of 1.4. The 1.4 scale factor was derived by comparing these three samples to well log values for V_P. Due to an insufficient number of samples, we were unable to develop scaling factors for different lithologies. These core plugs were tested unsaturated with the pore system drained to the atmosphere. Unfortunately, not a single sample or lithology is exposed to a full range of stresses, but a trend like that in Figure 3 is established using measurements from multiple core plugs. The data are noisy, but Figure 4 hints that core plugs with higher quartz percentage have higher velocities.

AVO and anisotropy

Rüger (2001) developed an expression for prestack reflection amplitudes from HTI media. To use Rüger's equation (equation 1), we measure reflection amplitudes as a function of the angle of incidence (θ) and source-receiver azimuth angle (ϕ). The output parameters include intercept (A_{iso}), isotropic gradient (B_{iso}), anisotropic gradient (B_{ani}) and azimuth of isotropy plane (ϕ_{iso}) at every time sample of every CDP (equation 1). These parameters may tell us about fractures if we assume 1) a model of an isotropic layer overlying an HTI medium (Rüger 1998), 2) the HTI anisotropy is caused by one dominant set of vertical fractures with strike direction parallel to ϕ_{iso}, and 3) B_{ani} represents the fracture density. Downton (2011) develops a theoretical relationship between HTI anisotropy and fractures by starting with the assumption that the fractures are penny-shaped (Hudson 1981). Downton (2011) also points out that it

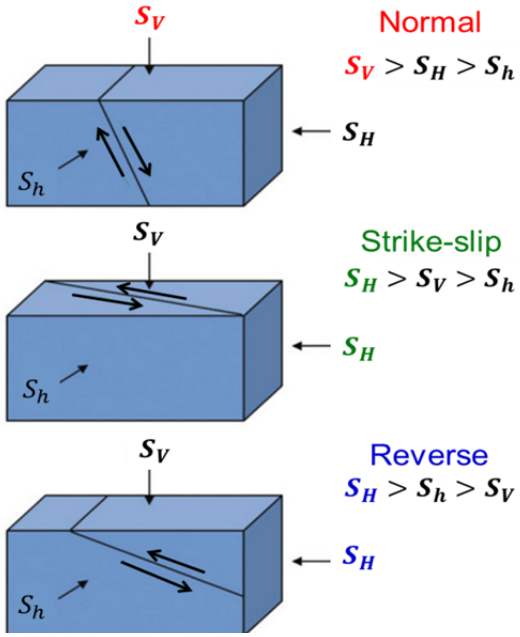

Figure 2: Figure adapted from Wikel (2011) showing Anderson (1951) fault classification system. The target formation is under transitional strike-slip and reverses fault regimes. Vertical fractures, if exist, will align conjugate to S_H direction.

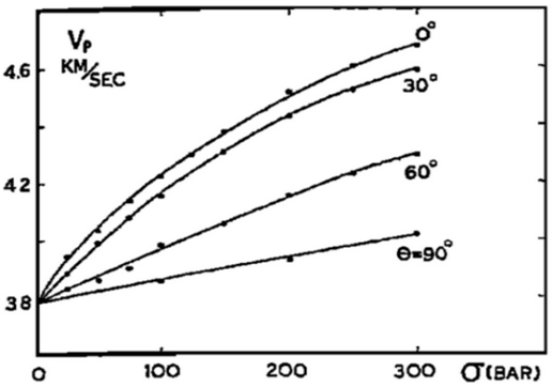

Figure 3: Nur and Simmons (1969) show V_P relationship with stress (σ) and direction of applied stress. θ represents angles between applied stress and direction of V_P Propagation. P-waves travel the fastest when parallel to the applied stress direction. At σ = 300 bars, the velocity parallel with stress direction (θ = 0°) increased by approximately 20%, while only 5% increase is observed in the perpendicular direction (θ = 90°).

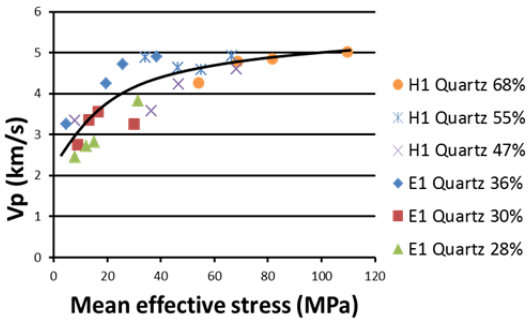

Figure 4: V_P dynamic versus the mean effective stress analyses over six unsaturated core plugs with varying quartz percentage. V_P increases with mean stress.

is not possible to know if anisotropic gradient is positive or negative, thus introducing 90° ambiguity to ϕ_{iso}.

$$R(\theta,\phi) = A_{iso} + [B_{iso} + B_{ani} sin^2(\phi - \phi_{iso})] sin^2\theta \quad (1)$$

Shaw and Sen (2006) came up with another equation to model azimuthal reflectivity as Fourier Coefficients (F.C.) series (equation 2), using the parameters r_0, r_2, r_4, incidence angle (θ) and source-receiver azimuth angle (ϕ). Here ϕ_{sym} is the azimuth of symmetry axis, which is perpendicular to ϕ_{iso}. r_0 is an equivalent to the isotropic three-term AVO equation while B_{ani} information is a scaled r_2 term (Downton 2011). Both r_2 and r_4 terms contain information on tangential and normal fracture weaknesses (Downton 2011). These fracture weaknesses describe how much strain of the fractured rock system is taken up by the fractures (Delbecq, et al. 2013, Downton 2011).

$$R_{pp}(\phi,\theta) = r_0 + r_2 \cos\left(2(\phi - \phi_{sym})\right) + r_4 cos\left(4(\phi - \phi_{sym})\right) \quad (2)$$

HTI velocity anisotropy can be measured on 3D seismic data by two different methods: 1) anisotropic migration velocities (Taylor, et al. 2013), and 2) azimuthal AVO (Downton and Roure 2010, Gray and Head 2000). We report results from both methods below. Our interval velocities are from a time migration and Dix inversion. A case study from 3D land survey in New Zealand reported high differential horizontal stress has resulted in significant velocity anisotropy of about 5% to 10% (Taylor, et al. 2013).

Other authors have discussed theoretical means to determine if velocity anisotropy is stress or fractures induced (Nur 1971, Schoenberg and Sayers 1995). Franco, et al. (2006) used dipole shear sonic logs to estimate the magnitude and azimuth of anisotropy induced by stress, intrinsic (preferred crystal orientations in shales) and extrinsic anisotropy (fractures) by measuring the shear wave splitting, shear wave travel time and analyzing flexural wave dispersion curves. With this study, instead of a theoretical approach, we compare seismic-derived anisotropy to a 'ground truth' from dipole sonic logs, borehole breakout and fractures interpreted from image logs to determine if the seismic anisotropy is stress or fracture induced.

METHOD AND RESULTS

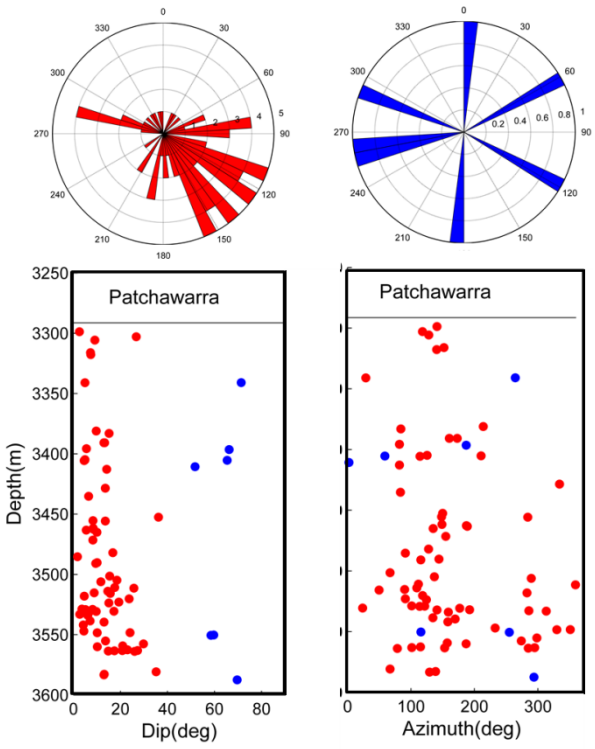

Figure 5: Image log natural fractures interpretation from a well within the study area. Shallowly dipping fractures (red) are abundant, whereas steeply dipping fractures (blue) are scarce.

Image logs analysis

Out of three image logs available within the 3D seismic survey, only one has adequate resolution for fracture interpretation. The well in this study is a vertical well with borehole deviation less than 1°. Fracture and stress interpretation was conducted over the Patchawarra Formation. From 57 borehole breakouts (BO) observed on sand intervals, mean current $\boldsymbol{S_H}$ direction was found to be N100°E. In contrast, no drilling-induced tensile fractures (DITF) were observed. Fracture interpretation results indicate many shallowly dipping (<50°) fractures (similar to beds) while the occurrence of steeply dipping (>50°) fractures are scarce (<10 over 300m interval) (Figure 5). Most of these fractures are oriented SE-NW, which is about 30° conjugate to current $\boldsymbol{S_H}$. This orientation is expected under the current Cooper Basin strike-slip stress regime (Anderson 1951, Healy, et al. 2006, King, et al. 2011).

The horizontal or near horizontal fractures cannot cause seismic anisotropy (both AVO anisotropy and HTI velocity anisotropy). The scarcity of steeply dipping fractures in these image logs suggests that fractures are not the cause of the observed seismic anisotropy.

Image log data over the shale intervals show neither fractures nor BOs. The conventional wisdom of wellbore failure suggests that BOs occur in weak shales rather than stiffer sandstones. However, in the Cooper Basin and some other basins in Australia, BOs are more common in sandstones (King, et al. 2011, Nelson, et al. 2006). This can be explained by the Nelson, et al. (2006) stress-partitioning model that reveals sandstones act as a stress-bearing unit when subjected to high horizontal stresses. The combination of low-stress concentration and the absence of fractures and BOs, shales are predicted to have a low potential for HTI anisotropy.

Dipole shear log and core analysis

Dipole sonic logs from nearby wells show high anisotropy in shear velocity (V_S) in sands (10-16%) and coals (1 to 10%) (Figure 6). Both sand and coal dipole anisotropy are consistently oriented around N100°E, which matched with interpreted present-day S_H orientation from earlier BOs analysis. Shale has less than 1% anisotropy with no specific orientation. The high-stress concentration on sand and cleats or conchoidal fractures in coal may be responsible for the high anisotropy. Low anisotropy in shales suggests little or no fractures. Furthermore, stress-partitioning model mentioned earlier mean that shale does not experience high differential stress, hence low anisotropy.

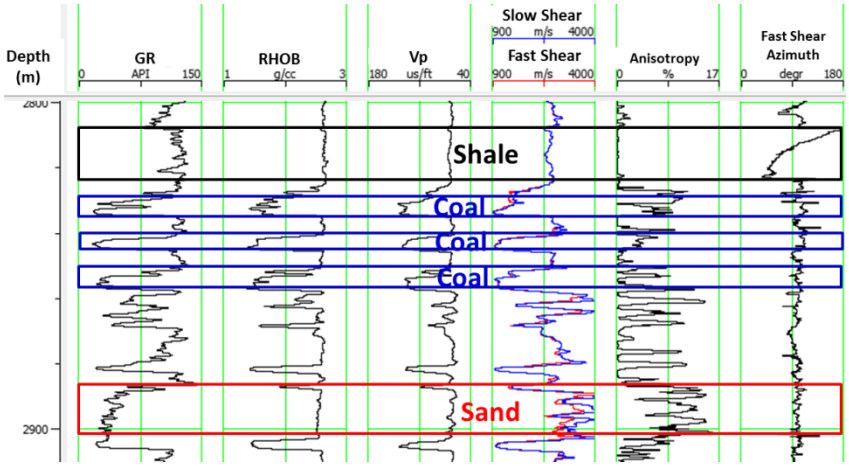

Figure 6: Well log showing gamma ray (GR), density (RHOB), V_P, fast shear, slow shear, anisotropy and fast shear azimuth. The difference between fast and slow V_S provides an estimate of anisotropy magnitude. High anisotropy occurs in sand and coal not shale.

To investigate the possible causes of anisotropy seen on dipole shear log, we inspected the core for fractures and cleats. Core data over sand intervals reveals minimal vertical fractures but abundant horizontal 'disking' (similar to fractures), spaced a few mm apart and often seen cross-cutting each other. It is unclear if this disking occurs in the subsurface or is an artifact of the coring process. Even if disking does occur in the subsurface, it is unlikely to show up on the dipole sonic log as the disking has no vertical component.

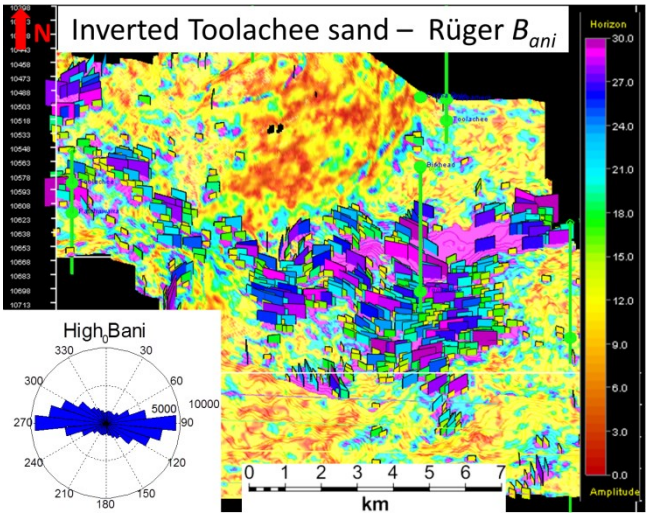

Figure 7: Inverted Toolachee sand map of Rüger anisotropic gradient (B_{ani}). Rectangular plate size, colour and direction represent the magnitude of B_{ani} and orientation of isotropy plane (ϕ_{iso}). Colour bar represents both the background surface and the rectangular plates. A rose plot on the bottom left corner shows ϕ_{iso} orientation, which is parallel to stress orientation.

Coal intervals display many conchoidal fractures (vertical and horizontal) with no preferred orientation. However, the dipole sonic indicates N102°E as preferred fast shear direction. We speculate that this anisotropy is supported by current day S_H, which has kept the E-W vertical fractures in coal open.

Shale intervals are homogenous with no visible fractures. The combination of low-stress concentration predicted earlier, and the absence of fractures correspond well with the low shear anisotropy signature in shales.

Azimuthal AVO (AVA) analysis

Input data are fully azimuthal gathers with a maximum offset of 6.8km, which were migrated using a proprietary VTI-HTI time migration algorithm. Analysis of the migrated gathers show poor signal-to-noise ratio (S/N) at a far offset (45°), and an outer angle mute was applied to remove those angles.

A relative inversion was performed on real seismic data. The AVO attribute maps shown here were extracted from the horizon picked on relative inverted data. We applied AVO lithologic constraints created from V_P, V_S and density log to stabilize the inversion results.

We performed azimuthal AVO inversion with lithologic constraints using Rüger (2001) near offset approximation

(equation 1) and the FCs (equation 2) and compared the relative anisotropy magnitude (B_{ani} - Rüger and r_2 – FC) and azimuth (ϕ_{iso}). Results show agreement on the location of high anisotropy in pink and major anisotropy orientation of approximately N95°E, which is aligned with S_H (Figure 7 and Figure 8).

Migration velocity analysis

Similar to the above AVA analysis, the magnitude and azimuth of the migration velocities were extracted over the Toolachee sand. The ratio or the difference between fast and slow shear interval velocities to the fast shear velocity was used as a measure of anisotropy. After muting out artifacts at the survey edges, the results show that most of the fast shear data are oriented approximately N100°E, which is parallel with current S_H (Figure 9).

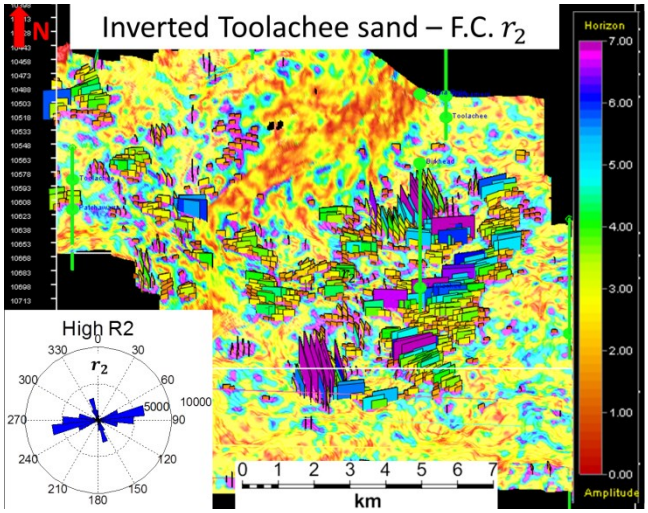

Figure 8: Inverted Toolachee sand map of Fourier Coefficient scaled anisotropic gradient (r_2). Rectangular plate size, colour and direction represent the magnitude of r_2 and orientation of isotropy plane (ϕ_{iso}). Colour bar represents both the background surface and the rectangular plates. High anisotropy area agrees with area shown in Figure 7. The ϕ_{iso} orientation shown on rose diagram at the bottom left is more varied than Rüger ϕ_{iso} orientation.

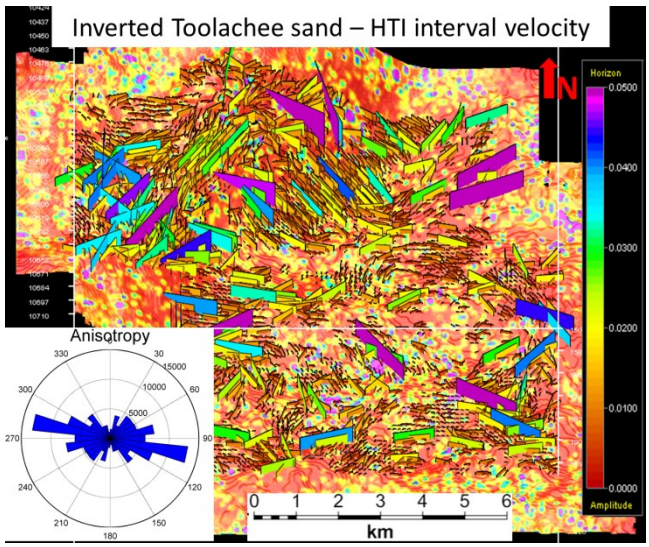

Figure 9: Inverted Toolachee sand map of migration velocity anisotropy (1-Vslow/Vfast) after muting data around the edges. The rectangular plate size, colour and direction represent the magnitude and orientation of velocity anisotropy. Colour bar represents both the background surface and the rectangular plates. Rose diagram shows that azimuth of HTI velocity anisotropy is aligned with current S_H direction.

CONCLUSIONS

Large differential stress and vertical fractures may cause azimuthal HTI anisotropy. The Cooper Basin 3D seismic data exhibit this HTI anisotropy in both amplitude (AVO) and interval migration velocity. The magnitude and orientation of AVO seismic anisotropy are measured using near offset Rüger and Fourier Coefficient algorithms. The results from anisotropic AVO maps and HTI interval migration velocity over Toolachee sand show that the anisotropy is oriented N100°E, which is aligned with the Cooper Basin's regional S_H.

Theory predicts that vertical natural fractures created by the Cooper Basin strike-slip stress environment will be oriented approximately 30° from S_H. Image log analyses show none of the vertical natural fractures are aligned with S_H. The fact that the seismic anisotropy is aligned with S_H and not with the observed fractures suggests that differential stress is responsible for the anisotropy observed on Cooper seismic data.

ACKNOWLEDGMENTS

Financial support for this work came from the GeoFrac sponsors at the Australian School of Petroleum, University of Adelaide. Those sponsors include Santos Ltd., Beach Petroleum, QGC/BG, Halliburton, and Chevron. Assistance with software licenses was provided by CGG: Hampson-Russell, DownUnder Geosolutions, and IkonScience: JRS Suite

REFERENCES

Anderson, E.M., 1951, The Dynamics of Faulting and Dyke Formation with Applications to Britain: Hafner Pub. Co.

Delbecq, F., Downton, J.E., and Letizia, M., 2013, A Math-Free Look at Azimuthal Surface Seismic Techniques: CSEG Recorder, **38**, 20-31.

Downton, J.E., Azimuthal Fourier Coefficients: A Simple Method to Estimate Fracture Parameters: SEG Annual Meeting, SEG.

Downton, J.E., and Roure, B.2010,Azimuthal Simultaneous Elastic Inversion for Fracture Detection: 2010 SEG Annual Meeting.

Franco, J.L.A., Ortiz, M.A.M., De, G.S., Rentie, L., and Williams, S., 2006, Sonic Investigations in and around the Borehole: Oilfield Review, **18**, 14-33.

Gray, D., and Head, K., 2000, Fracture Detection in Manderson Field: A 3-D Avaz Case History: The Leading Edge, **19**, 1214-21.

Grechka, V., and Tsvankin, I., 1999, 3-D Moveout Velocity Analysis and Parameter Estimation for Orthorhombic Media: Geophysics, **64**, 820-37.

Greenstreet, C., and Dello, L., 2015, Santos and the Cooper Basin: The Next Frontier. Gas Today, Winter 2015, 76-78.
Healy, D., Jones, R.R., and Holdsworth, R.E., 2006, Three-Dimensional Brittle Shear Fracturing by Tensile Crack Interaction: Nature, **439**, 64-67.

Hudson, J.A., 1981, Wave Speeds and Attenuation of Elastic Waves in Material Containing Cracks: Geophysical Journal International, **64**, 133-50.

Jenner, E., 2011, Combining Vti and Hti Anisotropy in Prestack Time Migration: Workflow and Data Examples: The Leading Edge, **30**, 732-39.

King, R., Abul Khair, H., Bailey, A., Backé, G., Holford, S., and Hand, M., Integration of in-Situ Stress Analysis and Three-Dimensional Seismic Mapping to Understand Fracture Networks in Australian Basins: Australian Geothermal Energy Conference 2011129-34.

Mavko, G., Mukerji, T., and Godfrey, N., 1995, Predicting Stress-Induced Velocity Anisotropy in Rocks: Geophysics, **60**, 1081-87.

Nelson, E., Hillis, R.R., and Mildren, S.D., 2006, Stress Partitioning and Wellboure Failure in the West Tuna Area, Gippsland Basin: Exploration Geophysics, **37**, 215 - 21.

Nur, A., 1971, Effects of Stress on Velocity Anisotropy in Rocks with Cracks: Journal of Geophysical Research, **76**, 2022-34.

Nur, A., and Simmons, G., 1969, Stress-Induced Velocity Anisotropy in Rock: An Experimental Study: Journal of Geophysical Research, **74**, 6667-74.

Perez, M.A., and Gibson Jr, R.L., Detection of Fracture Orientation Using Azimuthal Variation of P-Wave Avo Responses: Barinas Field (Venezuela): 1996 SEG Annual Meeting, SEG.

Radke, B., 2009, Hydrocarbon & Geothermal Prospectivity of Sedimentary Basins in Central Australia; Warburton, Cooper, Pedirka, Galilee, Simpson and Eromanga Basins. in Geoscience (ed.): Geoscience Australia.

Reynolds, S.D., Mildren, S.D., Hillis, R.R., Meyer, J.J., and Flottmann, T., 2005, Maximum Horizontal Stress Orientations in the Cooper Basin, Australia: Implications for Plate-Scale Tectonics and Local Stress Sources: Geophysical Journal International, **160**, 331-43.

Rüger, A., 2001, Reflection Coefficients and Azimuthal Avo Analysis in Anisotropic Media: Society of Exploration Geophysicists.
Rüger, A., 1998, Variation of P-Wave Reflectivity with Offset and Azimuth in Anisotropic Media: Geophysics, **63**, 935-47.

Sarkar, D., Bakulin, A., and Kranz, R.L., 2003, Anisotropic Inversion of Seismic Data for Stressed Media: Theory and a Physical Modeling Study on Berea Sandstone: Geophysics, **68**, 690-704.

Sayers, C.M., and Rickett, J.E., 1997, Azimuthal Variation in Avo Response for Fractured Gas Sands: Geophysical Prospecting, **45**, 165-82.

Schoenberg, M., and Sayers, C.M., 1995, Seismic Anisotropy of Fractured Rock: Geophysics, **60**, 204-11.

Shaw, R.K., and Sen, M.K., 2006, Use of Avoa Data to Estimate Fluid Indicator in a Vertically Fractured Medium: Geophysics, **71**, C15-C24.

Taylor, R., Cordery, S., Nixon, S., and Driml, K., Unexpected Hti Velocity Anisotropy: A Wide-Azimuth, Low Fold, 3D Seismic Processing Case Study: ASEG-PESA 20131-5.

Thomsen, L., 1986, Weak Elastic Anisotropy: Geophysics, **51**, 1954 - 66.

Treadgold, G., Sicking, C., Sublette, V., and Hoover, G., 2008, Azimuthal Processing for Fracture Prediction and Image Improvement: CSEG recorder, **33**, 38-42.

Valcke, S.L.A., Casey, M., Lloyd, G.E., Kendall, J.M., and Fisher, Q.J., 2006, Lattice Preferred Orientation and Seismic Anisotropy in Sedimentary Rocks: Geophysical Journal International, **166**, 652-66.

Wikel, K., 2011, Geomechanics: Bridging the Gap from Geophysics to Engineering in Unconventional Reservoirs: First Break, **29**, 71-80.